JOURNAL OF CATALYSIS 87, 305–318 (1984)

Kinetics and Mechanism of Methanol Decomposition over Zinc Oxide

KHALID M. TAWARAH[1] AND ROBERT S. HANSEN[2]

Ames Laboratory, USDOE, Department of Chemistry, Iowa State University, Ames, Iowa 50011

Received September 9, 1982; revised December 22, 1983

The kinetics of CH_3OH decomposition over ZnO was studied in the temperature ranges 453–513 K and 563–613 K. In the first range, CH_3OH decomposed to H_2 and CH_2O, while in the second range CH_3OH decomposed to CH_2O, CO, CO_2, and H_2 with the CO and CO_2 probably formed through formaldehyde or formate intermediates. The initial rate of production of hydrogen, R_{H_2}, depended on the methanol pressure P_m according to $(P_m/R_{H_2})^{1/2} = a + bP_m$; the initial rate of production of carbon monoxide plus carbon dioxide, R_c, depended on P_m according to $(P_m/R_c)^{1/3} = c + dP_m$. Both R_{H_2} and R_c were independent of hydrogen, carbon monoxide, and carbon dioxide pressures over the temperature and pressure ranges studied. At 500 K and a given pressure, CH_3OH decomposed more rapidly than CH_2O. In both the low- and high-temperature ranges the decomposition of CH_3OH, CH_3OD, and CD_3OD follow $R_{CH_3OH} = R_{CH_3OD} > R_{CD_3OD}$. A mechanism accounting for these findings is presented. Principal features are $CH_3O_* + H_* \rightarrow H_2 + CH_2O_*$ followed by either $CH_2O_* \rightarrow CH_2O(g) + *$ (the only step observed at low temperature) or $CH_2O_* + * \leftrightarrows CHO_* + H_* \rightarrow CO + H_2$. The fraction of formaldehyde decomposing increases with T and is about 20% at 593 K.

INTRODUCTION

Methanol synthesis and decomposition over ZnO and promoted ZnO have received numerous investigations. High-pressure (*1–4*) and low-pressure (*5–7*) synthesis kinetic studies resulted in the proposal of several rate-determining steps. These include a trimolecular surface reaction (*1*), methanol desorption (*2*), hydrogen adsorption (*4*), a surface reaction involving a methoxy radical and adsorbed atomic hydrogen (*6, 7*), and the hydrogenolysis of the Cu–C bond on a copper-based catalyst (*8*). IR studies (*9, 10*) of the adsorption of CO on hydrogen-saturated surfaces have indicated the replacement of the Zn–H band at 1708 cm^{-1} by a triplet at lower frequencies, while the O–H band at 3498 cm^{-1} is shifted to higher frequencies. These observations were considered to establish CO–H_2 (D_2) interaction in the adsorbed state. A formyl species has also been reported, although the evidence for it is not strong (*11*). The mutual enhancement of the adsorption of CO and H_2 has been attributed to formation of a CHOH (*12, 13*) or CH_3O (*14*) complex. Studies in which H_2 was replaced by D_2 in the synthesis gas are conflicting. In one case (*6*) no isotopic effect was observed, while in another (*15*) a reverse kinetic isotope effect was reported.

Several investigations have appeared on methanol decomposition with emphasis on reaction kinetics (*16, 17*), effect of ZnO doping on the activation energy (*18–20*), or identification of surface species (*21*). Recent studies emphasizing temperature-programmed reaction spectroscopy (*22–26*) have provided strong evidence for a formate intermediate in the decomposition of methanol and formaldehyde on zinc oxide, and that the formate decomposition is the rate-limiting step in production of CO and CO_2. The formate is reported to result from nucleophilic attack on the formaldehyde

[1] Present address: Department of Chemistry, Yarmouk University, Irbid, Jordan.

[2] Author to whom correspondence should be addressed.

0021-9517/84 $3.00

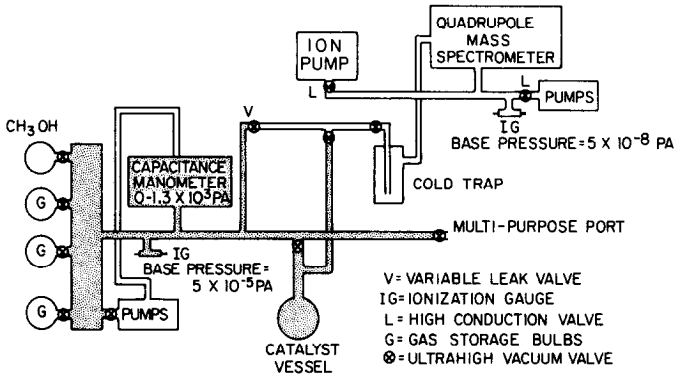

FIG. 1. Schematic of the vacuum system used in the kinetic study (shaded area = reaction volume = 2.04×10^{-3} m^3).

carbon by surface oxygen (*22–24*). Cheng *et al.* (*25*) studied the decomposition of CD_3OD on ZnO prismatic $(10\bar{1}0)$, polar (0001), and two-stepped $[4(10\bar{1}0) \times (0001)$, and $5(10\bar{1}0) \times (0001)]$ single-crystal ZnO surfaces, finding CO, CO_2, and D_2 produced in all cases, CD_4 also produced on prismatic and stepped surfaces but not on the polar surface, and CD_2O and D_2O also observed on the polar surface but not on the other surfaces. Bowker *et al.* (*26*) were unable to observe methanol decomposition on the prismatic ZnO single-crystal face, and concluded that catalytic activity for methanol decomposition must lie in the polar face.

A scheme of two first-order reactions, involving the intermediate formation of formaldehyde, was proposed long ago (*16, 17*); the adsorbed formaldehyde intermediate can be assigned structures consistent with the formate intermediate (*22–26*). Kinetic data in support of this mechanism have been limited with little pressure variation, and no quantitive rate equation consistent with such a mechanism has been developed.

In the present work, the dependence of the rate of decomposition of methanol over ZnO on methanol pressure was studied at low pressures using vacuum techniques, which made 100-fold variation in the pressure easily accessible.

EXPERIMENTAL

Apparatus and Procedures

A schematic of the vacuum system used in this study is shown in Fig. 1. The reaction enclosure (shaded area in Fig. 1) is connected to the mass spectrometer (Finnigan Spectroscan 400) via a leak valve, which allows continuous sampling of the gas phase during the course of an experiment. The manifold (shaded area in Fig. 1 excluding catalyst vessel) was used for admitting the required amount of reactant before expanding to the catalyst. A capacitance manometer, calibrated against a McLeod gauge, was used for pressure measurements. The catalyst vessel is a Pyrex flask with volume 9.75×10^{-4} m^3, of which 6.0×10^{-4} m^3 was at reaction temperature. The temperature of the catalyst vessel was monitored by the use of a chromel–alumel thermocouple. In order to eliminate the contribution of CH_3OH and/or CH_2O to the CO signal at $m/e = 28$, a trap was maintained at 195 K by a dry ice–acetone slush. The multipurpose port, shown in Fig. 1, was used for attaching to the vacuum system the McLeod gauge, standard volume, apparatus for handling CH_3OH, apparatus for handling the deuterated compounds, or the apparatus used for CH_2O preparation. The latter is similar to that of Spence and Wild (*27*). CH_3OH was purified by bulb-to-

bulb vacuum distillation and was loaded to the system as liquid. Hydrogen exchange between CH_3OD/CD_3OD and the walls of the system was observed. To eliminate this problem, the reaction enclosure including the catalyst were treated with D_2O. Several cycles of dosing and pumping out of D_2O vapor were carried out until the peak of $m/e = 17$ (OH) became negligible compared to $m/e = 18$. CH_3OD and CD_3OD were injected into a predeuterated handling apparatus and stored as vapor in a bulb attached to the vacuum system.

The flow reactor, used for testing CH_2O formation during CH_3OH decomposition, consisted of a vertical Pyrex tube (reactor), a 500-ml flask through which He gas was passed over boiling CH_3OH, and a conical flask containing distilled water. The effluent gas, after leaving the reactor, was passed through the conical flask to obtain an aqueous solution of CH_2O. The BET surface area of the catalyst was 3.0×10^3 m^2 kg^{-1} as established using an Orr surface area pore volume analyzer (Micromeritics Instruments Corp. Model 2100D) with N_2 adsorbate. The initial reactant pressure over the catalyst was calculated using an expansion factor of 0.60 in the range 453–623 K. Both methanol and CH_2O were found to adsorb to the walls of the system. To reduce errors resulting from back desorption, the contact time of the reactant vapor with the manifold walls was kept small (pressure drop $\ll$ 10%). Prior to a kinetic experiment, the catalyst was treated with about 67 Pa O_2 at the reaction temperature for all experiments at $T \leq 513$ K. For experiments at $T \geq 563$ K oxygen was admitted at 523 K. This was done in order to have a common oxygen treatment for the low- and high-temperature runs. In both cases, after admitting O_2, the catalyst temperature was raised to 623 K at a rate of 0.2 K s^{-1}. O_2 was then pumped out and heating was continued up to 673 K. Outgassing at this temperature lasted for 30 min. The temperature was then lowered to the reaction temperature. Mass spectrometric analysis of the gas phase over the catalyst at the end of the oxygen treatment revealed the presence of O_2, CO, CO_2, and H_2 as the major components. In the absence of oxygen pretreatment, the outgassing of the catalyst (after the termination of a methanol kinetic run), while increasing temperature up to 673 K, resulted in the formation of a Zn film especially for runs involving methanol pressures over 100 Pa. The oxygen treatment eliminated the catalyst reduction and resulted in fairly good experimental reproducibility. To check the sensitivity of kinetic data to oxygen pretreatment, the standard pretreatment was followed by a 10-min exposure to O_2 at a series of pressures $0 \leq P_{O_2} \leq 45$ Pa at 588 K, the O_2 pumped out for 10 min, 10.8-Pa CD_3OD admitted, and its initial decomposition rate measured. Rates of production of D_2, CO, and CO_2 were independent of the P_{O_2} used in the second pretreatment. The decomposition of CH_3OH and/or CH_2O was followed by monitoring peaks at $m/e = 2$ (H_2), $m/e = 28$ (CO), and $m/e = 44$ (CO_2). CO_2 contribution to $m/e = 28$ amounted to ~10% of the $m/e = 44$ signal. This was subtracted from the total $m/e = 28$ signal. CH_2O produced in CH_3OH decomposition was trapped, and so did not contribute to the mass 28 peak. Peaks at $m/e = 2$ (H_2), $m/e = 3$ (HD), and $m/e = 4$ (D_2) were used to determine the total initial hydrogen production from CH_3OD. HD calibration (Pa/mV signal) was obtained using the equilibrium constant for the reaction $H_2 + D_2 \rightleftarrows 2HD$ at ~298 K, taken as 3.28 (*28*). The exchange reaction (initial mixture: $H_2/D_2 = 1$) seemed to be catalyzed by some metal surface in the manifold. Rapid equilibration was attained after applying an electric field (Tesla coil). The initial rates were calculated from the initial rate of product partial pressure increase for times less than 120 s.

The formaldehyde was prepared by the thermal depolymerization of paraformaldehyde at ~350 K. The formaldehyde vapor was condensed at 195 K. It was then frozen at 77 K in order to pump out any CO and/or

H_2 that might have resulted during the preparation step. After this treatment the formaldehyde was stored at 195 K as liquid which was used as a source of gas monomeric CH_2O. A mass spectrum of the CH_2O vapor was recorded and revealed three peaks at m/e = 30, 29, and 28. No peaks higher than m/e = 30 were observed which is an indication of the absence of the potential impurities methyl formate and trioxane. The same spectrum can be obtained after several days provided that the separator and the receiving flask are kept at 195 K.

Materials

All of the gases used in the kinetic and isotopic studies were research grade gases. D_2, CO, CO_2, Ar, and O_2 were purchased from the Linde division of Union Carbide. H_2 was purchased from Matheson Gas Products and $^{13}C^{18}O$ (90% ^{13}C, 95% ^{18}O) was purchased from Prochem Isotopes. All gases were purchased in glass bulbs with breakable seals. Their purities were confirmed mass spectrometrically before use. D_2O (99.7%) was purchased from Merck & Company; chromotropic acid was purchased from Aldrich Chemical Company as a hydrated sodium salt. Paraformaldehyde was purchased from Fisher Scientific Company. CH_3OH (spectral quality) was obtained from Burdick & Jackson Laboratories, Inc. CH_3OD (>99.5%) and CD_3OD (99.5%) were obtained from the Alfa Division of Ventron Corporation. The three methanols gave mass spectra in agreement with those reported in Ref. (*29*) except that the abundance of the m/e = 28 fragment was ~4 times higher than reported in Ref. (*29*). This might be due to methanol decomposition on the hot filament of the ionizer assembly. The ZnO sample (SP500, 99.99% pure) was supplied by the New Jersey Zinc Company. The catalyst purity was checked by spectrographic and X-ray fluorescence analysis. No impurities exceeded 100 ppm; trace elements under 100 ppm included Fe, Cu, Mn, Pb, As, Cd, Al, Ca, Na, Si, and Mg. The amount of ZnO catalyst used in the kinetic study was 1.0×10^{-3} kg. All results were obtained on the same batch. Before being placed in the catalyst vessel, the ZnO sample was heat-treated at 823 K for 90 min. After this treatment, the catalyst was never subjected to temperatures higher than 673 K. The catalyst sample used was a fine powder having an average particle diameter of $\sim 4 \times 10^2$ nm.

RESULTS AND DISCUSSION

Temperature Dependence of CH_3OH Decomposition

Our initial CH_3OH decomposition experiments indicated a slow evolution of H_2 beginning at 423 K, and fast decomposition at 633 K. At the latter temperature production of H_2, CO, and CO_2 (and small amounts of H_2O and CD_4) was accompanied by Zn film formation on the cold part of the catalyst vessel. No CH_3OH homogeneous decomposition was detected up to 633 K. CO and CO_2 were found to be produced concurrently at T ~ 550 K. In the range 453–513 K negligible CO or CO_2 was produced over the experimental period (up to 15% CH_3OH present initially decomposed). This observation suggests that methanol decomposition is occurring in stages, as stated by Dohse (*16*) and strongly supported by the experiments of Cheng *et al.* (*25*).

The decomposition of CH_3OH was compared with that of CH_3OD in the temperature range 453–513 K. CH_3OD decomposition resulted in the formation of H_2, HD, and D_2. Furthermore, the initial rates of hydrogen production were the same for the two methanols. In the case of CH_3OD, the isotopic scrambling indicates that both the methyl and the hydroxyl groups are responsible for hydrogen production. The observation that both CH_3OH and CH_3OD have the same decomposition rates suggests that the dissociation of the hydroxyl hydrogen, during the adsorption step on the catalyst surface, is unlikely to be a rate-determining step. A similar remark has been made by McKee (*30*) for the decomposition of meth-

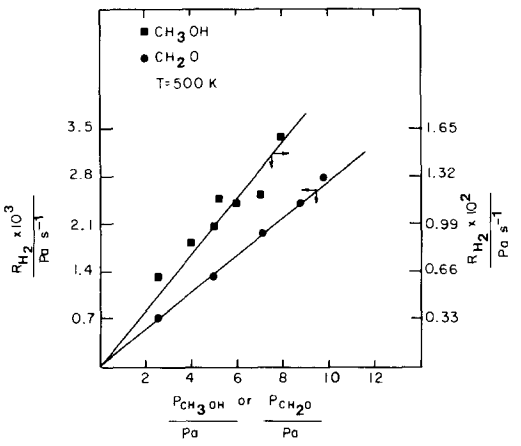

FIG. 2. Comparison between the initial rates of decomposition of CH_3OH and CH_2O over ZnO. Rate in Pa s^{-1} × 2.42 × 10^{-7} = rate in mol m^{-2} s^{-1}.

anol on Pt. The nonparticipation of the methyl hydrogen in the isotope exchange between CH_3OH and D_2 was reported on Ni (*31*), ZnO, and other metal films (*32*). Evidence and conclusions concerning the hydrogen isotope effect will be discussed in a later section.

Based on these observations, the kinetics of methanol decomposition was studied over two temperature ranges: 453–513 K, and 563–613 K. The first range was chosen for studying the kinetics of H_2 production, while the second range was chosen for studying the kinetics of CO and CO_2 production.

Detection of CH_2O

Although the intermediate formation of CH_2O during the homogeneous (*33*) and heterogeneous decomposition (*16*) of methanol has long been reported, several researchers made no mention of CH_2O (*21, 34*). In our study, formation of CH_2O via the catalytic decomposition of CH_3OH on ZnO was confirmed for both flow and static reactors. In the case of the flow reactor, the effluent gas was passed through distilled water. Addition of chromotropic acid, as suggested in Ref. (*35*), to the test solution resulted in the formation of a purple color, which is indicative of the presence of CH_2O. Formation of CH_2O was confirmed at 523 and 573 K.

Formation of CH_2O in the high vacuum system (static reactor) was confirmed mass spectrometrically. Warming up the trap resulted in a mass spectrum having the ratio h (m/e = 29)/h (m/e = 31) > 1. The ratio is <1 for CH_3OH.

Comparison between Decomposition and Uptake of CH_3OH and CH_2O

The decomposition of CH_2O was compared with that of CH_3OH on the same batch of ZnO catalyst at 500 K. Figure 2 indicates that CH_3OH decomposed about 7 times faster than CH_2O at the same pressure. This result fits well with the observation that, during CH_3OH decomposition in the range 453–513 K, no carbon oxides were detected during the 2-min experiments used for measurement of initial reaction rates, although up to 15% of the CH_3OH in the system had reacted. At 500 K CH_3OH decomposition produced H_2 and CO in a 1 : 1 ratio and no CO_2 was detected.

Figure 3 illustrates initial uptake of both CH_3OH and CH_2O by ZnO at 500 K. In this figure, the abscissa represents the initial pressure of CH_3OH or CH_2O over the catalyst at the moment vapor was admitted

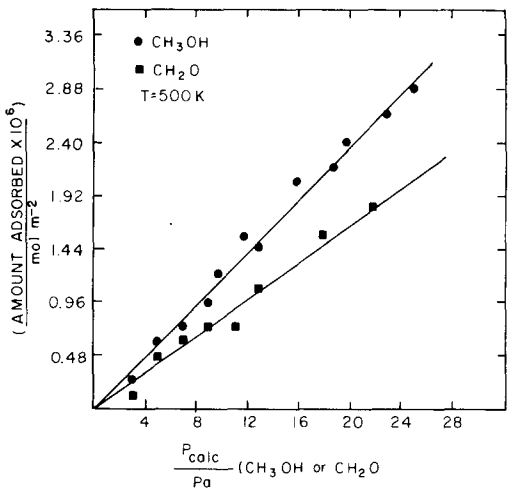

FIG. 3. Comparison between CH_2O and CH_3OH initial uptake by ZnO.

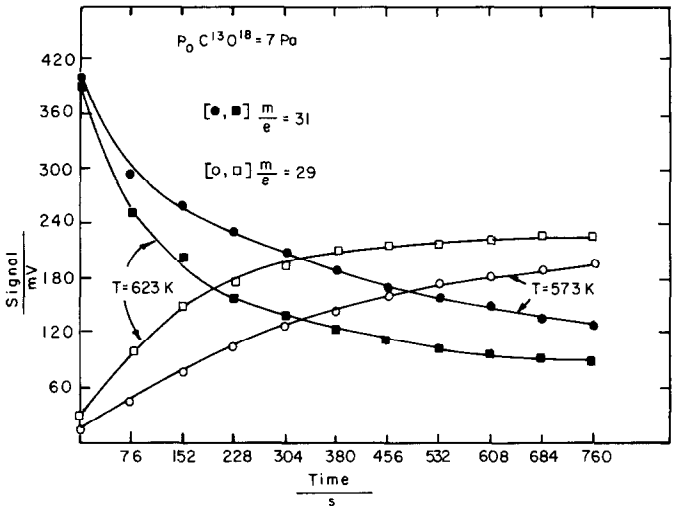

FIG. 4. Oxygen exchange between $^{13}C^{18}O$ and $Zn^{16}O$.

from the manifold to the catalyst vessel. P(calc) was determined from knowledge of the expansion factor assuming no adsorption by the catalyst. The ordinate represents the initial uptake of vapor by ZnO = $F \cdot \Delta P$, where $F = 2.42 \times 10^{-7}$ mol m^{-2} Pa^{-1}, and $\Delta P = [P(\text{calc}) - P_0]$ Pa; P_0 was determined by extrapolating the total pressure over the catalyst to zero reaction time. Because the rate of adsorption was fast compared to the rate of reaction, the amount adsorbed could be estimated from the difference in calculated and measured pressures at a time sufficiently short that negligible reaction had occurred. The difference in the uptake might be attributed to a difference in the ratio $P(\text{calc})/P_s$, where P_s = saturation vapor pressure. Since the boiling point of CH_3OH is higher than that of CH_2O, the ratio is much higher for CH_3OH than for CH_2O at a particular adsorption temperature.

Interaction of CO with ZnO

In an attempt to identify the path by which CO_2 is produced during CH_3OH decomposition, the interaction of CO with ZnO was examined under conditions similar to those encountered in a CH_3OH decomposition experiment. The results of the $^{13}C^{18}O$ interaction at 573 and 623 K are shown in Fig. 4. No CO_2 was detected. These results can be explained if the following oxygen exchange reaction is assumed:

$$^{13}C^{18}O_{(g)} + Zn^{16}O_{(s)} = Zn^{18}O_{(s)} + {}^{13}C^{16}O_{(g)}. \quad (1)$$

The fact that no peak was detected at m/e = 47 ($^{13}C^{18}O^{16}O$) is an indication that CO_2 was not being produced in these experiments. Oxygen exchange between ZnO and CO has been reported by Carnisio *et al.* (*36*). ^{18}O placed on the ZnO surface in this way was not removed by several $^{16}O_2$ treatments at 623 K. Based on this observation the oxygen exchange between $^{13}C^{18}O$ and $Zn^{16}O$ was exploited to enrich the catalyst surface with ^{18}O for further experiments.

The ^{18}O-enriched ZnO was treated with the usual O_2 cleaning procedure, and $^{12}C^{16}O$ admitted to a pressure of 7.1 Pa at 570 K. Over a 10-min experiment the $^{12}C^{16}O$ gas concentration steadily decreased, that of $^{12}C^{18}O$ steadily increased, that of background $^{12}C^{16}O_2$ remained constant, and no $^{12}C^{16}O^{18}O$ was detected. Hence, under the conditions of our experiment, there was no detectable oxidation of CO by oxygen of the ZnO or by oxygen of a second CO mole-

cule (to leave C on the surface). Our results, showing no reduction of ZnO by CO, conflict with those of Hotan *et al.* (*37*) who reported that CO desorbs as CO_2 from ZnO. Bowker *et al.* (*24*) interpret the chemisorption of CO on ZnO as a reaction of CO with a surface O^- ion to form a surface CO_2^- ion. This reaction and its reverse also provide an interpretation of our findings.

Interaction of O_2 and H_2 with ^{18}O Enriched ZnO

The ^{18}O-enriched ZnO was treated with 66 Pa $^{16}O_2$ at 623 K for 2 h. Besides the major peak at m/e = 32 ($^{16}O_2$), the mass spectrum revealed small amounts of $^{16}O^{18}O$, $^{13}C^{16}O$, $^{12}C^{18}O$, $^{12}C^{16}O_2$, $^{13}C^{16}O_2$, and $^{12}C^{18}O^{16}O$. The absence of the species $^{13}C^{16}O^{18}O$, $^{13}C^{18}O_2$, and $^{13}C^{18}O$ implies that no $^{13}C^{18}O$ was left in a molecular form on the catalyst after evacuating $^{13}C^{18}O$ at 623 K prior to the admission of $^{16}O_2$. Formation of the other carbon oxides might be attributed to the reaction of oxygen with a $^{13}C/^{12}C$ deposit which might have resulted from exposure of ZnO to CH_3OH and $^{13}C^{18}O$ prior to the oxygen treatment. This result also demonstrates the value of the O_2 treatment after each methanol decomposition experiment for removing possible carbon residues.

The ^{18}O-enriched ZnO was also exposed to 6.3 Pa H_2 at 623 K for 17 min. The decrease in $P(H_2)$ amounted to ~8% of the initial pressure, or about 4×10^{-7} moles H_2. The absence of $H_2{}^{16}O$ and $H_2{}^{18}O$ peaks together with the absence of Zn deposit rule out a catalyst reduction by H_2.

Decomposition of CH_3OH over ^{18}O-enriched ZnO

Since the interaction of both $^{13}C^{18}O$ and $^{12}C^{16}O$ with ZnO did not result in the formation of any CO_2 under conditions similar to those encountered in CH_3OH decomposition, the CO_2 observed in CH_3OH decomposition must result from decomposition of

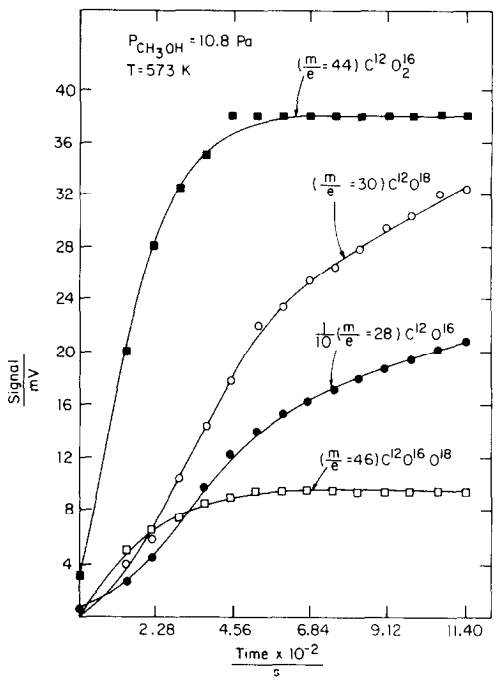

FIG. 5. Formation of carbon oxides during CH_3OH decomposition on ^{18}O-enriched ZnO.

a surface species formed by interaction of CH_3OH with ZnO. This might be a formate intermediate with the extra oxygen coming from ZnO. Participation of ZnO to produce CO_2 during CH_3OH decomposition is plausible if, during the course of CH_3OH decomposition over ^{18}O-enriched ZnO, the gas phase species $^{12}C^{16}O^{18}O$ and $^{12}C^{18}O$, together with the expected $^{12}C^{16}O$ and $^{12}C^{16}O_2$, are obtained. The result shown in Fig. 5 confirms the supposition that the formation of CO_2 requires oxygen participation from the ZnO lattice, probably via a formate intermediate. The experiment of Fig. 5 was terminated after about 50% carbon conversion into carbon oxides. CO_2 amounted to 20% carbon conversion. From knowledge of the total surface area of the catalyst and assuming that the surface atom density of the oxide ions = 5×10^{14} atom cm^{-2}, the fraction of the surface oxygen removed as CO_2 is 0.08. Similar results were obtained for CD_3OD decomposition over $Zn^{16}O$.

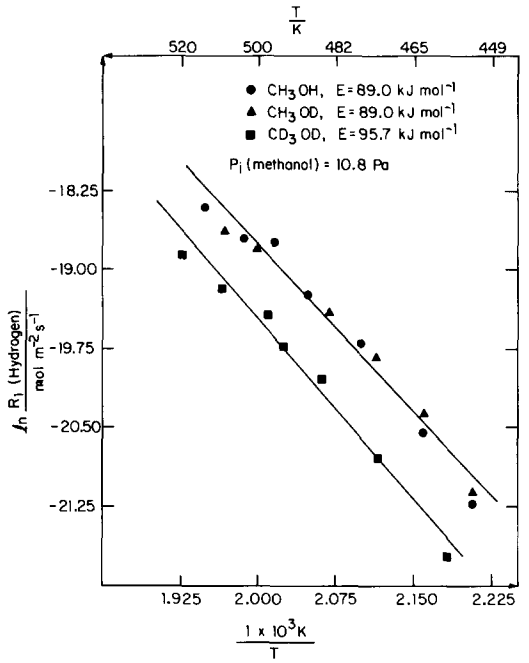

FIG. 6. Hydrogen isotope effect and apparent energies of activation for the decomposition of CH_3OH, CH_3OD, and CD_3OD over ZnO. Ordinate corresponds to the dehydrogenation step into formaldehyde and hydrogen.

The leveling off of CO_2 production, despite the continuous evolution of CO, may be due to charge and vacancy accumulation on the catalyst due to consumption of the oxide ions. Hotan *et al.* (*37*) used a similar explanation for the variation in ZnO surface conductivity, after admission of CO.

Evolution of CO_2, during methanol decomposition on ZnO and promoted ZnO, has been reported by Tsuchiya and Shiba (*34*), Uchida and Ogino (*38*), Kung and coworkers (*25, 39*), and Ueno *et al.* (*21*).

H Isotope Effect and Apparent Activation Energies

The fact that no CO and/or CO_2 were produced initially up to ~550 K and the detection of CH_2O below and above 550 K have led to the conclusion that methanol decomposition on ZnO proceeds overall in two steps as suggested by Dohse (*16*), namely,

$$CH_3OH_{(g)} \rightarrow CH_2O_{(g\text{ or ad})} + H_{2(g)} \quad \text{(step 1)}, \quad (2)$$

$$CH_2O_{(g\text{ or ad})} \rightarrow CO_{(g)} + H_{2(g)} \quad \text{(step 2)}. \quad (3)$$

The kinetics of the first step was studied at 453–513 K, while the kinetics of both steps was studied at 563–613 K. The decomposition of CH_3OH, CH_3OD, and CD_3OD was studied in the two temperature ranges as shown in Figs. 6 and 7. Figure 6 suggests that cleavage of a carbon–hydrogen bond is a rate-determining step in the dehydrogenation of methanol to hydrogen and formaldehyde (low T decomposition). Formation of H_2, HD, and D_2 during low T decomposition of CH_3OD (HD dominating) is evidence against the model proposing that hydrogen comes solely from the hydroxyl group. Participation of the methoxy group is required, probably via steps accomplishing the reaction

$$CH_3O_* + D_* \rightarrow CH_2O_{(g)} + HD_{(g)} + 2_* \quad (* = \text{surface site}). \quad (4)$$

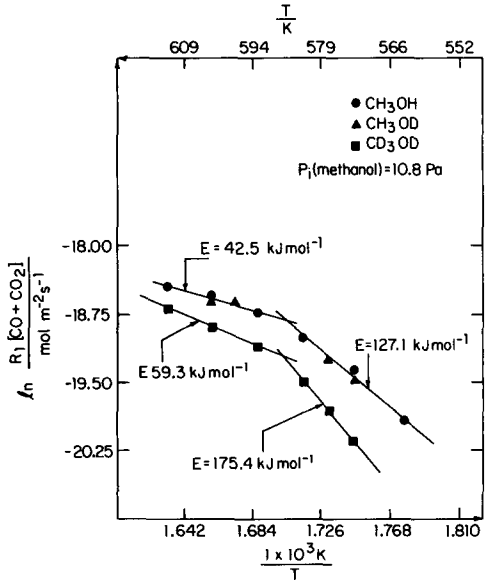

FIG. 7. Temperature dependence of the initial rates of total carbon oxides production. Ordinate corresponds to the second step of methanol decomposition.

The observed isotopic scrambling likely occurred on manifold walls as discussed under apparatus and procedures; ZnO is also known to catalyze H_2–D_2 isotopic mixing (*40*).

In the high T range, where evolution of CO and CO_2 is observable, the initial rate of step 2 in methanol decomposition is assumed to be the sum of CO and CO_2 production rates. Figure 7 indicates that both CH_3OH and CH_3OD decompose at the same rate, while CD_3OD decomposes at a slower rate. This implies that the formaldehyde hydrogen is totally originating from the methyl hydrogen of the parent methanol molecule. On this basis both CH_3OH and CH_3OD should give the same formaldehyde, i.e., CH_2O. Again the kinetic isotope effect, evident in Fig. 7, suggests that the rate-determining step of formaldehyde decomposition involves cleavage of a hydrogen–carbon bond.

Figure 7 shows a bend at ~590 K. Such a break in the Arrhenius plot for the methanol decomposition has been reported by several investigators (see Ref. (*41*) and references therein for various explanations of this break). A comment on this break is given later in the mechanistic considerations section.

Effect of $P(H_2)$ and $P(CO_2)$ on CH_3OH Decomposition

The effect of hydrogen pretreatment on CH_3OH decomposition at 500 K was checked by treating the ZnO with H_2 at various pressures from 0 to 21 Pa at 500 K for 5 min at each pressure, pumping out the hydrogen for 5 min, then measuring the initial rate of decomposition of CH_3OH at 500 K and initial pressure 9.8 Pa. The rate was independent of the hydrogen pretreatment pressure. Dependence of initial CH_3OH decomposition rate at 593 K was investigated by codosing 4.6-Pa CH_3OH and various H_2 pressures, and measuring rates of H_2, CO, and CO_2 production. All production rates were found to be zero order in P_{H_2}, P_{CO}, and P_{CO_2} up to pressures of at least 15 Pa at 563 K. Readsorption of the products H_2, CO, and/or CO_2 hence negligibly affects the decomposition under the reaction conditions investigated.

The apparent activation energy of CH_3OH decomposition in the range 453–513 K is 89.0 kJ mol^{-1}. The activation energy for H_2 desorption on a powder sample of ZnO at $T \leq 550$ K was found to be ~22 kJ mol^{-1} (*42*). Hence H_2 desorption is unlikely to be a rate-determining step in CH_3OH decomposition. A similar conclusion holds for CO and CO_2 desorption when the apparent energy of activation of CH_3OH decomposition in Fig. 9 (127.1 kJ mol^{-1} up to ~590 K) is compared with the value 90 ± 10 kJ mol^{-1} of the activation energy for CO_2 or CO desorption on ZnO (*37*).

Effect of $P(CH_3OH)$ on the Initial Rates

The low T CH_3OH decomposition, where no carbon oxides were formed, was studied by monitoring H_2 production at 500 K with the initial pressure of CH_3OH ranging from 2 to 31 Pa. The initial rate of H_2 production, $R(H_2)$, was determined from the amount of H_2 produced during the first 120 s of reaction. The dependence of $R(H_2)$ on the initial CH_3OH pressure was found to satisfy

$$[P(CH_3OH)/R(H_2)]^{1/2} = a + bP(CH_3OH). \quad (5)$$

The fit of the data to this equation is shown in Fig. 8. Values of the constants for the best least squares fit shown were a = 12.4 $s^{1/2}$ and $b = 1.7\ s^{1/2}\ Pa^{-1}$.

The high T CH_3OH decomposition, where H_2 and carbon oxides were being produced, was studied at 593 K with $P(CH_3OH)$ ranging from 3 to 130 Pa. The initial rates were determined from the amount of product produced in 60 s. The initial rate of evolution of carbon oxides, R_c, was obtained by summing those for CO and CO_2. $R(H_2)$, which corresponds to the first step of CH_3OH decomposition, was obtained by subtracting R_c from the initial

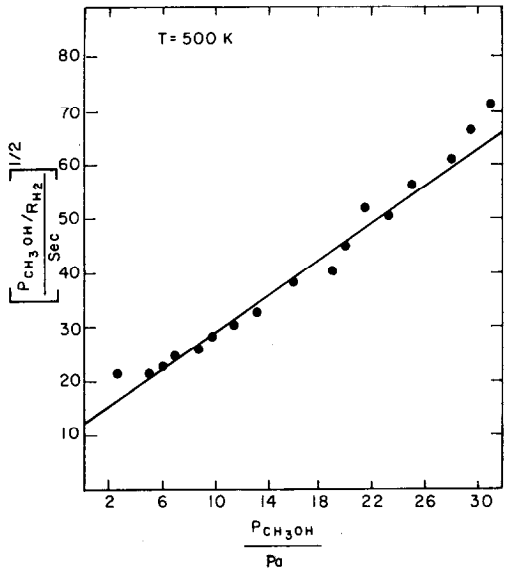

FIG. 8. Fit of the low temperature CH_3OH decomposition data to the equation $[P(CH_3OH)/R(H_2)]^{1/2} = a + bP(CH_3OH)$.

rate of total hydrogen production. The dependence of $R(H_2)$ on $P(CH_3OH)$ was found to satisfy Eq. (5) reasonably well, with $a = 6.44\ s^{1/2}$ and $b = 0.55\ s^{1/2}\ Pa^{-1}$. The dependence of R_c on $P(CH_3OH)$ could be similarly represented, but could be slightly better represented by

$$[P(CH_3OH)/R_c]^{1/3} = c + dP(CH_3OH). \quad (6)$$

The two plots are compared in Fig. 9; the plot according to Eq. (6) is preferred because of the systematic positive curvature evident in the plot according to Eq. (5) at low $P(CH_3OH)$.

Despite the presence of a cold trap at 195 K, between the leak valve and the mass spectrometer, CH_3OH peaks started to appear in the mass spectrum at $P(CH_3OH) >$ 130 Pa, which interfered with CO analysis. Due to this limitation, CH_3OH decomposition at $P(CH_3OH) > 130$ Pa was not studied further. Nevertheless, it was possible to vary the initial $P(CH_3OH)$ by two orders of magnitude, permitting a reasonable test of kinetic mechanisms.

MECHANISTIC CONSIDERATIONS

Consider the following sequence of reactions:

$$CH_3OH_{(g)} + * \overset{K_1}{\rightleftarrows} CH_3OH_* \quad \text{(step 1)}, \quad (7)$$

$$CH_3OH_* + * \overset{K_2}{\rightleftarrows} CH_3O_* + H_* \quad \text{(step 2)}, \quad (8)$$

$$CH_3O_* + H_* \overset{k_3}{\rightarrow} CH_2O_* + H_{2(g)} + * \quad \text{(step 3)}, \quad (9)$$

$$CH_2O_* \overset{k_4}{\rightarrow} CH_2O_{(g)} + * \quad \text{(step 4)}, \quad (10)$$

$$CH_2O_* + * \overset{K_5}{\rightleftarrows} CHO_* + H_* \quad \text{(step 5)}, \quad (11)$$

$$CHO_* + H_* \overset{k_6}{\rightarrow} H_{2(g)} + CO_{(g)} + 2* \quad \text{(step 6)}. \quad (12)$$

Formation of CO_2 can be understood if step 6 proceeds through a formate intermediate; the following scheme is patterned after the scheme in Ref. (*24*):

$$CHO_* + O^- \rightarrow HCO_{2*}^-, \quad (13)$$

$$HCO_{2*}^- + H_* \overset{k_6}{\rightarrow} H_{2(g)} + CO_{(g)} + O^- + 2_* \quad (14a)$$

$$\overset{k_6'}{\rightarrow} H_{2(g)} + CO_{2(g)} + V + e + 2*, \quad (14b)$$

where V denotes a vacancy. Reaction (14b) creates vacancies and increases the number of electrons in the solid band system, which should tend to inhibit the reaction.

The steady decrease with time of the CO_2/CO ratio in the product gas is consistent with this interpretation. The initial rate

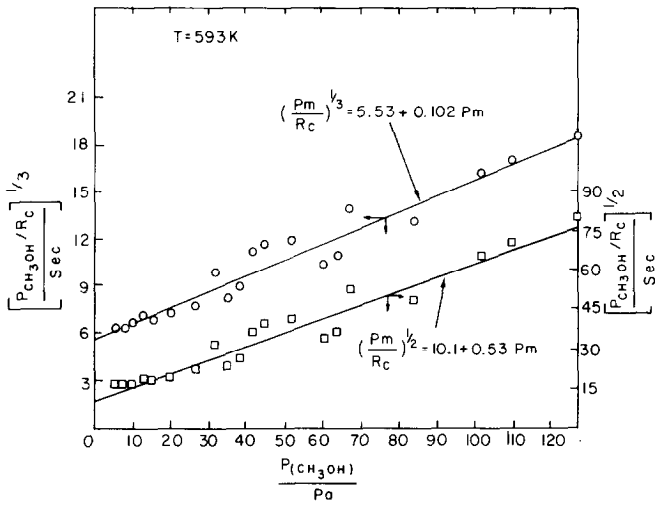

FIG. 9. Plot of $[P(CH_3OH)/R_c]^{1/3}$ and with $[P(CH_3OH)/R_c]^{1/2}$ vs $P(CH_3OH)$.

of production of carbon oxides R_c is given as

$$\begin{aligned} R_c &= R(CO) + R(CO_2) \\ &= (k_6 + k_6')[CHO^*][H^*] \\ &= k_c[CHO^*][H^*] \\ &= k_c K_5[CH_2O^*][*]. \end{aligned} \quad (15)$$

Steps 3 and 6 are taken as irreversible because over the pressure and temperature ranges investigated the reaction rate was found to be zero order in the hydrogen and carbon monoxide partial pressure. Step 4 is taken as irreversible because no evidence of poisoning of rate by $[CH_2O^*]$ build up was observed. As a simplifying attack on this set of equations we suppose all other steps in the mechanism are approximately at equilibrium in steady state, express surface concentrations in coverage fractions, and suppose that all coverage fractions except (CH_3OH^*) are small compared to 1. Then the fractional coverage of empty sites follows from

$$1 = [*] + [CH_3OH_*] = [*](1 + K_1P_m), \quad (16)$$

i.e.,

$$[*] = (1 + K_1P_m)^{-1}. \quad (17)$$

The rate of production of hydrogen (and CH_2O^*) in step 3 is then

$$\begin{aligned} R_{H_2} &= k_3[CH_3O_*][H_*] \\ &= k_3K_2K_1P_m[*]^2 \quad (18) \\ &= k_3K_2K_1P_m[1 + K_1P_m]^{-2}. \quad (19) \end{aligned}$$

Equation (19) can be transformed into the form

$$[P_m/R(H_2)]^{1/2} = (k_3K_2K_1)^{-1/2} + K_1(k_3K_2K_1)^{-1/2}P_m. \quad (20)$$

Equation (20) has the same functional form as Eq. (5).

The $[CH_2O_*]$ is formed in step 3 at the same rate as hydrogen is formed in that step, and is removed (in steady state) as fast as it is formed by desorption as formaldehyde (step 4) or by decomposition to carbon monoxide (or carbon dioxide) and hydrogen via steps 5 and 6. For steady state, therefore, moles H_2 formed in step 3 = moles CH_2O desorbed in step 4 + moles CH_2O decomposed in step 6, i.e.,

$$k_3K_2K_1P_m[1 + K_1P_m]^{-2} = k_4[CH_2O_*] + k_cK_5[CH_2O_*][*] \quad (21)$$

whence

$$[CH_2O_*] = k_3K_2K_1P_m(1 + K_1P_m)^{-2}\{k_4 + k_cK_5(1 + K_1P_m)^{-1}\}^{-1}, \quad (22)$$

$$R_{CH_2O_{(g)}} = k_4k_3K_2K_1P_m(1 + K_1P_m)^{-2}\{k_4 + k_cK_5(1 + K_1P_m)^{-1}\}^{-1}, \quad (23)$$

$$R_c = k_c K_5 k_3 K_2 K_1 P_m (1 + K_1 P_m)^{-3} \{k_4 + k_5 (1 + K_1 P_m)^{-1}\}^{-1}, \quad (24)$$

so that $R_{CH_2O_{(g)}} + R_c = R_{H_2}$ from step 3 as required. At low temperature CO production is not observed; this implies that at low temperature $k_4 \gg k_c K_5 (1 + K_1 P_m)^{-1}$. According to this mechanism, at low pressure the quantity $k_c K_5 / k_4$ must increase with increasing temperature from a negligible value at 500 K to an appreciable value (about 0.25) at 593 K. Let $\alpha = k_c K_5 / k_4$, and for simplicity neglect $\alpha (1 + K_1 P_m)^{-1}$ compared to unity. Then Eq. (24) reduces to

$$R_c = \alpha k_3 K_2 K_1 P_m [1 + K_1 P_m]^{-3}. \quad (25)$$

This can be rearranged to

$$(P_M / R_c)^{1/3} = (\alpha k_3 K_2 K_1)^{-1/3} [1 + K_1 P_m] \quad (26)$$

which has the same functional form as Eq. (6). From Eqs. (19) and (26) it follows that

$$R_{H_2} / R_c = (1 + K_1 P_m) / \alpha. \quad (27)$$

Equation (27) represented R_{H_2} and R_c data at 593 K quite well.

Values of parameters calculated using Eqs. (20), (26), and (27) were reasonably self-consistent. Thus, K_1 can be obtained from the ratio of slope to intercept using any one of these equations; at 593 K we find $10^2 K_1/\text{Pa} = 1.99$ (Eq. (20)), 1.84 (Eq. (26)), and 1.57 (Eq. (27)). From Eq. (27) we find at 593 K $\alpha = 0.246$. Using this with $\alpha k_3 K_2 / P_a$ $s^{-1} = 0.32$ obtained by the plot from Eq. (26) we obtain $k_3 K_2 / P_a = 1.30$ which is comparable with the value 1.21 obtained from the plot of Eq. (20).

The breaks in the Arrhenius plots shown in Fig. 7 would be expected from Eq. (25), but from parameters documented in this work would have been expected to occur at a somewhat lower temperature. Thus from Eq. (31) we obtain

$$R/E_{app} = -\left[\frac{\partial \ln R_c}{\partial (1/T)}\right]_{P_m} = \frac{(E_c^* + E_3^* - E_4^* + \Delta H_2 + \Delta H_1 + \Delta H_5)}{R} - \frac{3K_1 P_m}{1 + K_1 P_m} \frac{\Delta H_1}{R}. \quad (28)$$

From values of K_1 at 500 and 593 K we estimate $\Delta H_1 = -57$ kJ/mole. For $P_m = 10.8$ Pa as in Fig. 7 we calculate $K_1 P_m = 1.48$ at 500 K and 0.19 at 593 K. The last term in Eq. (28) hence increases the activation energy by 103 kJ at 500 K, but only by 28 kJ at 593 K. The shift is in the right order of magnitude, but occurs between $500 < T < 593$ K rather than in the range $565 < T < 609$ K covered by Fig. 7. Qualitatively, Eq. (28) predicts a high-temperature limiting slope corresponding to decomposition on a catalyst whose surface is negligibly blocked by adsorbed methanol, a low-temperature limiting slope corresponding to a catalyst whose surface is fully blocked by adsorbed methanol (so that methanol must be desorbed to provide sites for the reaction to proceed) and a corresponding difference in limiting apparent activation energies of 3 ΔH_1 or -171 kJ/mole. A similar analysis can be applied to the initial hydrogen-producing step 3 of the mechanism (Eq. (19) and Fig. 6); in this case the difference in limiting activation energies should be -2 ΔH, or -114 kJ. Although the data in Fig. 6 have been interpreted via linear plots the data points in all cases show a systematic negative curvature consistent with this interpretation. Intuitively, one would expect the apparent break in plots of ln R against $10^3/T$ to occur near $K_1 P_m = 1$ (about 517 K, $10^3/T = 1.94$ rather than near $10^3/T = 1.70$, $T = 588$ K as in Fig. 7); the appearance of the break at higher temperature in Fig. 7 may reflect a change in structure of adsorbed methanol at higher temperature. Conceivably appreciable fractions of the surface may be occupied by other species, e.g., (CH_2O_*) at higher temperatures; an analysis retaining (CH_2O_*) as an appreciable surface species was carried out, leading

to modifications of Eqs. (19) and (35) more complex in form with an additional adjustable parameter and little improvement in data representation. Finally, the quantity $\alpha = k_c K_5/k_4$, negligible at 500 K and approx 0.25 at 593 K, may increase further with temperature so that the approximation $[1 + \alpha(1 + K_1 P_m)^{-1}]^{-1} \approx 1$ used in reducing Eq. (24) to Eq. (25) is not justified at temperatures above 593 K. Further conjectures on the character of the break in Fig. 7 are not justified by data obtained in the present work.

Our mechanism proposes that at low T the ZnO surface sites are either bare or occupied by a species treated formally as molecularly adsorbed CH_3OH, with negligible coverage by other surface species. The apparent importance of polar ZnO surfaces in CH_3OH decomposition catalysis (*25, 26*) suggests conjecture as to sites and adsorption modes in terms of these polar surfaces. Both Zn and O are tetrahedrally coordinated in the zincite structure. The polar planes can be envisioned as containing an outside layer of atoms of one kind, each missing a partner above it in the direction perpendicular to the plane but possessing its other three neighbors in the other three tetrahedral directions. These latter atoms lie in a second plane below the outer plane; all atoms in this plane are of the second kind, and each has its full complement of four neighbors (in a perfect unreconstructed structure). The outermost layer can be either all Zn atoms or all O atoms; we shall denote these (0001) and (000$\bar{1}$) surfaces, respectively. How might the methoxide and formate species, widely documented by IR studies of CH_3OH adsorption on metal oxides (*43–47*) form on these surfaces? As initial models, we consider structures generated by coordinating a methoxy group to the most available Zn atom, the direction from Zn atom to the methoxy oxygen being perpendicular to the crystal plane surface with bond distance equal to the nearest neighbor ZnO distance in zincite. Data for this consideration are taken from Pauling (*48*). On the (0001) surface the methoxy group can be easily accommodated. The distance between methoxy oxygen and the nearest oxygens in the ZnO structure exceeds the van der Waals distance by about 0.04 nm and (choosing the Zn–O–C bond angle to be tetrahedral) the methyl group can be positioned so as to exceed the van der Waals distance by about 0.01 nm. The methyl group would, however, be hindered from rotating freely about the axis established by the bond between Zn and methoxy oxygen. The distance between methoxy oxygen and nearest oxygens in the ZnO structure exceeds the spacing between oxygen atoms hydrogen bonded in solid methanol by about 0.06 nm. It appears feasible to adsorb methanol in a similar structure with methanol oxygen hydrogen bonded to an oxygen in the ZnO structure by tilting the coordination vector from Zn to methanol oxygen about 25° from the surface normal. Evidently such a structure could readily lead to a transfer of a hydrogen atom to the oxygen atom in the zinc oxide structure and coordination of the methoxy group to a Zn atom in the manner previously described.

On the (000$\bar{1}$) surface similar bonding of a methoxy group to a Zn atom leads to distances between methoxy oxygen and nearest oxygens in the ZnO structure 0.05 nm *less* than the van der Waals distance, so the structure would be seriously crowded. However, the Zn atom in this case already had its full complement of four oxygen atoms before the methoxy group was added, and hence the bond to the methoxy oxygen would be expected to be weaker and its length greater than on the (0001) surface.

In either case, the species CH_3O_* is envisioned as CH_3O Zn, with the Zn atom coordinated to either 3 or 4 other oxygens, and the species H_* as HO, with the oxygen coordinated to 4 or 3 Zn atoms on the (0001) and (000$\bar{1}$) surfaces, respectively. Splitting out of hydrogen could then be rationalized as a combination of a proton (from the HO) with a hydride ion (from CH_3) with the in-

termediate carbonium ion stabilized by coordination to a second oxygen in the ZnO surface structure. The products are hence $H_{2(g)}$ and $H_2CO_{2(s)}$, the two oxygens (one of which came from the methanol, the other from the ZnO) both coordinated to Zn. $H_2CO_{2(s)}$ is hence a model for CH_2O_*, its formation corresponds to step 3 of the mechanism, and its decomposition to step 6; the products of the decomposition are H_2 and either CO or CO_2 (Eq. (14a) or (14b)) with a vacancy left in the latter case.

ACKNOWLEDGMENTS

This work was supported by the U.S. Department of Energy under Contract W-7405-Eng-82. Gratitude is expressed to Yarmouk University, Irbid, Jordan for a scholarship granted to K.M.T.

REFERENCES

1. Natta, G., *in* "Catalysis" (P. H. Emmett, Ed.), Vol. 3, Chap. 8. Reinhold, New York, 1955.
2. Uchida, H., and Ogino, Y., *Bull. Chem. Soc. Japan* **31,** 45 (1958).
3. Pasquon, I., *Chim. Ind.* **42,** 352 (1960).
4. Leonov, V. E., Karabaev, M. M., Tsybina, E. N., and Petrishcheva, G. S., *Kinet. Katal.* **14,** 970 (1973).
5. Cherednichenko, V. M., and Temkin, M. I., *Z. Fiz. Khim.* **31,** 1072 (1957).
6. Saida, T., and Ozaki, A., *Bull. Chem. Soc. Japan* **37,** 1817 (1964).
7. Borowitz, J. L., *J. Catal.* **13,** 106 (1969).
8. Herman, R. G., Klier, K., Simmons, G. W., Finn, B. P., Bulko, J. B., and Kobylinski, T. P., *J. Catal.* **56,** 407 (1979).
9. Dent, A. L., and Kokes, R. J., *J. Phys. Chem.* **73,** 3781 (1969).
10. Boccuzzi, F., Garrone, E., Zecchina, A., Bossi, A., and Camia, M., *J. Catal.* **51,** 160 (1978).
11. Saussey, J., Lavalley, J., Lamotte, J., and Rais, T., *J. Chem. Soc. Chem. Commun.* 278 (1982).
12. Nagarjunan, T. S., Sastri, M. V. C., and Kuriacose, J. C., *J. Catal.* **2,** 223 (1963).
13. Aharoni, C., and Tompkins, F. C., *Trans. Faraday Soc.* **66,** 434 (1970).
14. Tsuchiya, S., and Shiba, T., *J. Catal.* **4,** 116 (1965).
15. Belysheva, T. V., Shub, F. S., and Temkin, M. I., *Kinet. Katal.* **19,** 661 (1978).
16. Dohse, H., *Z. Phys. Chem.* **8B,** 159 (1930).
17. Tamura, M., *Rev. Phys. Chem. Japan* **16,** 71 (1942).
18. Menold, R., *Chem. Ing. Tech.* **32,** 801 (1960).
19. Dandy, J. A., *J. Chem. Soc.* 5956 (1963).
20. Fuderer-Luetic, P., and Sviben, I., *J. Catal.* **4,** 109 (1965).
21. Ueno, A., Onishi, T., and Tamaru, K., *Trans. Faraday Soc.* **67,** 3585 (1971).
22. Barteau, M. A., Bowker, M., and Madix, R. J., *Surface Sci.* **94,** 303 (1980).
23. Bowker, M., Houghton, H., and Waugh, K. C., *J. Chem. Soc. Faraday Trans. I* **77,** 3023 (1981).
24. Bowker, M., Houghton, H., and Waugh, K. C., *J. Chem. Soc. Faraday Trans. I* **78,** 2573 (1982).
25. Cheng, W. H., Akhter, S., and Kung, H. H., *J. Catal.* **82,** 341 (1983).
26. Bowker, M., Houghton, H., Waugh, K. C., Giddings, T., and Green, M., *J. Catal.* **84,** 252 (1983).
27. Spence, R., and Wild, W., *J. Chem. Soc.* 338 (1935).
28. Jones, T., and Sherman, A., *J. Chem. Phys.* **5,** 375 (1937).
29. Beynon, J. H., Fontaine, A. E., and Lester, G. R., *Int. J. Mass Spect. Ion Phys.* **1,** 1 (1968).
30. McKee, D. W., *Trans. Faraday Soc.* **64,** 2200 (1968).
31. Yasumori, I., Nakamura, T., and Miyazaki, E., *Bull. Chem. Soc. Japan* **40,** 1372 (1967).
32. Anderson, J. R., and Kemball, C., *Trans. Faraday Soc.* **51,** 966 (1955).
33. Fletcher, C. J. M., *Proc. Roy. Soc. London* **147,** 119 (1934).
34. Tsuchiya, S., and Shiba, T., *J. Catal.* **6,** 270 (1966).
35. Bricker, C. E., and Vail, W. A., *Anal. Chem.* **22,** 720 (1950).
36. Carnisio, G., Garbassi, F., Petrini, G., and Parravano, G., *J. Catal.* **54,** 66 (1978).
37. Hotan, W., Haul, R., and Gopel, W., *Surface Sci.* **83,** 162 (1979).
38. Uchida, H., and Ogino, Y., *Bull. Chem. Soc. Japan* **29,** 587 (1956).
39. Cheng, W. H., and Kung, H. H., *Surface Sci.* **102,** L21 (1981); "Book of Abstracts," 183rd National Meeting of ACS, Las Vegas, Nevada, March 1982, COLL 249.
40. Dixon, L. T., Dent, A. L., Chang, C. C., and Kokes, R. J., *J. Amer. Chem. Soc.* **94,** 4429 (1972).
41. Morrelli, F., Giorgini, M., Guerrini, R., and Tartarelli, R., *J. Catal.* **27,** 471 (1972).
42. Baranski, A., and Galuszka, J., *J. Catal.* **44,** 259 (1976).
43. Greenler, R. G., *J. Chem. Phys.* **37,** 2094 (1962).
44. Kagel, R. O., *J. Phys. Chem.* **71,** 844 (1967).
45. Thornton, E. W., and Harrison, P. G., *J. Chem. Soc. Faraday Trans. I* **71,** 2468 (1975).
46. Unland, M. L., *J. Phys. Chem.* **82,** 580 (1978).
47. Nagao, M., and Morimoto, T., *J. Phys. Chem.* **84,** 2054 (1980).
48. Pauling, L., "The Nature of the Chemical Bond," 3rd ed. Cornell Univ. Press, Ithaca, N.Y., 1960.